

Impacts of Assimilating Measurements of Different State Variables with a Simulated Supercell Storm and Three-Dimensional Variational Method

GUOQING GE

Center for Analysis and Prediction of Storms, University of Oklahoma, Norman, Oklahoma

JIDONG GAO

National Severe Storm Laboratory, Norman, Oklahoma

MING XUE

Center for Analysis and Prediction of Storms, and School of Meteorology, University of Oklahoma, Norman, Oklahoma

(Manuscript received 10 July 2012, in final form 17 January 2013)

ABSTRACT

This paper investigates the impacts of assimilating measurements of different state variables, which can be potentially available from various observational platforms, on the cycled analysis and short-range forecast of supercell thunderstorms by performing a set of observing system simulation experiments (OSSEs) using a storm-scale three-dimensional variational data assimilation (3DVAR) method. The control experiments assimilate measurements every 5 min for 90 min. It is found that the assimilation of horizontal wind \mathbf{V}_h can reconstruct the storm structure rather accurately. The assimilation of vertical velocity w , potential temperature θ , or water vapor q_v can partially rebuild the thermodynamic and precipitation fields but poorly retrieves the wind fields. The assimilation of rainwater mixing ratio q_r can build up the precipitation fields together with a reasonable cold pool but is unable to properly recover the wind fields. Overall, \mathbf{V}_h data have the greatest impact, while q_v have the second largest impact. The impact of q_r is the smallest. The impact of assimilation frequency is examined by comparing results using 1-, 5-, or 10-min assimilation intervals. When \mathbf{V}_h is assimilated every 5 or 10 min, the analysis quality can be further improved by the incorporation of additional types of observations. When \mathbf{V}_h are assimilated every minute, the benefit from additional types of observations is negligible, except for q_v . It is also found that for \mathbf{V}_h , w , and q_r measurements, more frequent assimilation leads to more accurate analyses. For q_v and θ , a 1-min assimilation interval does not produce a better analysis than a 5-min interval.

1. Introduction

Numerical weather prediction (NWP) of severe thunderstorms is very important for saving lives and properties. To get a good prediction of thunderstorms, the initial condition from which a forecast starts is expected to be as accurate as possible. In recent years, much research has been done to improve initial conditions for storm-scale NWP. There are generally two ways to do so: 1) develop and improve NWP models and data assimilation

techniques to make the best use of available observations and background information, and 2) design and deploy additional high-resolution observing systems to improve the quality and coverage of atmospheric observations.

Currently, Doppler radars can routinely provide one component of the storm-scale three-dimensional wind field (radial velocity). The full horizontal wind field can be retrieved to some degree of accuracy using multiple Doppler radars, provided good multi-Doppler coverage can be obtained. Rainfall information (rainwater mixing ratio, snow water mixing ratio, hail mixing ratio) can be derived from observed radar reflectivity (including dual-polarization observations), satellite imagery data, and surface cloud reports. In the future, it is expected that

Corresponding author address: Dr. Guoqing Ge, Center for Analysis and Prediction of Storms, Suite 2500, 120 David L. Boren Blvd., Norman, OK 73072.
E-mail: geguoqing@ou.edu

the vertical velocity field will be observed in high resolution by spaceborne or airborne high-frequency Doppler radar. The water vapor field can be derived at high resolution from next-generation Geostationary Operational Environmental Satellite (GOES) observations, radar refractivity observations, and observations by a dense network of ground-based global positioning system (GPS) receivers. The temperature field can also be profiled in high resolution by next-generation GOES.

Even as more data assimilation and observing system studies are performed, some fundamental questions remain to be answered. What are the impacts of assimilating measurements of various state variables on storm analysis and short-range forecast? How does the model respond to the assimilation of individual types of measurements? How quickly can a quality initial condition be obtained using intermittent data assimilation? Will more frequent assimilation (rapid updates) necessarily yield good results?

Weygandt et al. (1999) performed experiments to study the relative importance of different data fields in a numerically simulated convective storm by sequentially withdrawing information from each model variable and rerunning the simulation. The perturbation horizontal velocity was found to have the greatest influence on the evolution of the simulated convective storm. Park and Droegemeier (2000) examined the sensitivity of a supercell storm simulation to errors in model fields in the context of four-dimensional variational data assimilation. They concluded that the forecast error is most sensitive to the inaccuracy of temperature, followed by pressure and water vapor. Weygandt et al. (2002a,b) conducted several sensitivity tests and found that their supercell storm simulation was greatly dependent on initial moisture fields, especially the water vapor field. Sun (2005) studied the relative importance of different initial fields on the forecast of an observed supercell storm by resetting a given initial field to its base state. Wind, water vapor, and temperature perturbation fields showed the largest sensitivities. Nascimento and Droegemeier (2006) examined, using an idealized simulation of a bow-echo convective system, the nature of the dynamic adjustment that occurred after resetting a given model data field to its base state. Horizontal wind fields were found to be crucial for an accurate simulation. Fabry and Sun (2010) and Fabry (2010) studied the propagation of initial condition errors in mesoscale convections using four-dimensional variational data assimilation (4DVAR), finding that error in midlevel moisture (humidity) has the greatest impact on the quality of the forecast. Zhang et al. (2004) conducted some sensitivity tests on the observing frequency and data coverage for convective-scale data assimilation

using an ensemble Kalman filter (EnKF). They found that low-level observations are important for the capture of the storms and that frequent observations can improve the data assimilation in the early stage (during the first half-hour). Tong and Xue (2005) studied the impact of radial velocity and radar reflectivity on the data assimilation for an idealized supercell thunderstorm using EnKF, finding that the best results are obtained when both types of data are assimilated into the model.

All the above studies contribute to our understanding of the relative importance of different state variables for mesoscale/storm-scale data assimilation and prediction. However, because of their different contexts and different focuses, there are differences among the conclusions of these studies. These differences call for more research on this issue. Furthermore, the manner in which model fields adjust at the storm scale in response to the assimilation of different observations after a cold start is not explicitly investigated. In this study, we perform more than a dozen idealized experiments to study the impact of assimilating measurements of different state variables on storm-scale analyses and short-range forecasts in the context of a three-dimensional variational data assimilation (3DVAR) system. Unlike the data-denial method or sensitivity method used in many previous studies (e.g., Weygandt et al. 1999; Sun 2005; Nascimento and Droegemeier 2006), we will examine the relative importance of different data fields by assimilating the measurements of them into the model. For each observing system simulation (OSS) data assimilation experiment, we examine whether it can successfully reproduce the storm structures (dynamic, thermodynamic, and precipitation structures), how long is required to achieve a successful recovery, and how accurate are the final analyses. The impact of assimilation frequency will also be examined.

This paper is organized as follows: section 2 will cover the methodology and the design of experiments, section 3 will discuss the results from these experiments, and conclusions will be provided in section 4.

2. Methodology and experimental design

a. *The 3D variational formulation*

Based on Bayesian probability theory and assuming Gaussian error distributions, Lorenc (1986) derived the standard formulations of the variational data assimilation problem. A variational method determines the optimal analysis by directly minimizing a cost function. The cost function of the Advanced Regional Prediction System (ARPS; Xue et al. 2000, 2001, 2003) 3DVAR system (Gao et al. 2004) is written as

$$J(\mathbf{X}) = J_B + J_O + J_C = \frac{1}{2}(\mathbf{X} - \mathbf{X}_b)^T (\mathbf{B}^{-1})(\mathbf{X} - \mathbf{X}_b) + \frac{1}{2}[H(\mathbf{X}) - \mathbf{y}_o]^T \mathbf{R}^{-1}[H(\mathbf{X}) - \mathbf{y}_o] + J_C, \quad (1)$$

where J_B measures the departure of the analysis \mathbf{X} from the background \mathbf{X}_b , and is weighted by the inverse of the background error covariance matrix \mathbf{B} ; J_O measures the departure of $H(\mathbf{X})$, the projection of the analysis \mathbf{X} into observational space, from observations \mathbf{y}_o and is weighted by the inverse of the observational error covariance matrix \mathbf{R} . The quantity J_C is the penalty or equation constraint term, which can be used to build linkages among model variables by using the mass continuity equation and/or a diagnostic pressure equation (Ge et al. 2012).

Although equation constraints can help spread observation information to some unobserved model variables, they also complicate the data impact problem. This study focuses on the data impact of individual model fields or their combinations, as well as the model response from cold start to the ingestion of observations; therefore, in this study, J_C is not used. Furthermore, in this study, pseudo-observations are directly drawn from the model variables, so no projection or interpolation is needed. These conditions result in a simpler cost function:

$$J(\mathbf{X}) = J_B + J_O = \frac{1}{2}(\mathbf{X} - \mathbf{X}_b)^T \mathbf{B}^{-1}(\mathbf{X} - \mathbf{X}_b) + \frac{1}{2}(\mathbf{X} - \mathbf{X}_o)^T \mathbf{B}^{-1}(\mathbf{X} - \mathbf{X}_o). \quad (2)$$

The goal of obtaining an analysis is to find a state \mathbf{X}_a for which J is minimized. At its minimum, the derivative of J becomes zero; therefore, the cost function of \mathbf{X}_a satisfies $\nabla J(x) = \mathbf{B}^{-1}(\mathbf{X} - \mathbf{X}_b) + \mathbf{R}^{-1}(\mathbf{X} - \mathbf{X}_o) = 0$. In the ARPS 3DVAR system (Gao et al. 2004), the background error covariance \mathbf{B} is assumed to be spatially homogeneous with isotropic Gaussian spatial correlations. The actual effects of \mathbf{B} are realized through recursive filters (Purser and McQuigg 1982; Hayden and Purser 1995) as described in Gao et al. (2004). The error variances for each of the state variables will be provided in the next section. It is realized that this \mathbf{B} is not flow dependent, as is the case with most 3DVAR systems. As a result, the assimilation of observations of individual state variables may not be as effective as would be the case when using other more advanced data assimilation methods such as EnKF and 4DVAR, where the covariance \mathbf{B} is explicitly or implicitly flow dependent. In the current 3DVAR systems, dynamic consistency among the state variables is achieved mostly through model adjustment during the high-frequency assimilation cycles. Given that the main goal of this study is to investigate the

relative importance of the measurements of different state variables, the conclusions should not depend too much on the assimilation method.

b. The prediction model and truth simulation

In this study, we use simulated data from a classic supercell storm on 20 May 1977 in Del City, Oklahoma (Ray et al. 1981). The ARPS system is used to simulate this storm within a $64 \text{ km} \times 64 \text{ km} \times 16 \text{ km}$ physical domain comprising $67 \times 67 \times 35$ grid points. Horizontal grid spacing of 1 km and vertical grid spacing of 0.5 km are used, with the first scalar model level located at 250 m above ground level (AGL). The truth simulation is run for 3 h, and is initialized from a modified real sounding plus a +4-K ellipsoidal thermal bubble centered at $x = 48 \text{ km}$, $y = 16 \text{ km}$, and $z = 1.5 \text{ km}$, with radii of 10 km in the x and y directions and 1.5 km in the vertical direction. The Kessler (1969) warm rain microphysical scheme is used together with a 1.5-order turbulent kinetic energy-based subgrid parameterization. Open conditions are used at the lateral boundaries and a wave radiation boundary condition is applied at the top boundary. A free-slip boundary condition is applied at the bottom. A constant wind of $u = 3 \text{ m s}^{-1}$ and $v = 14 \text{ m s}^{-1}$ is subtracted from the observed sounding to keep the primary storm cell near the center of model domain.

The evolution of the simulated storms is similar to that documented in Xue et al. (2001) and is shown in Fig. 1. The initial convective cell strengthens over the first 20 min and begins to split into two cells at around 55 min. The right-moving cell is dominant, traveling north-northeastward while remaining near the center of domain. The left-moving cell travels northwestward, reaching the northwest corner of the domain 2 h into the simulation.

c. Experimental design

After creating the truth simulation of the tornadic thunderstorms, pseudo-observations are directly taken from the simulated model state variables. The pseudo-observations used are horizontal wind \mathbf{V}_h , vertical velocity w , potential temperature θ , water vapor mixing ratio q_w , and rainwater mixing ratio q_r . Gaussian noise is added to the above data fields to mimic observation error. The standard deviations for the error fields of the observations σ_o and the background σ_b are given in Table 1.

Pseudo observations are collected from the truth simulation between 30 and 120 min after it is initialized. The assimilation experiments start with a horizontally homogeneous background initialized using the same sounding used in the truth run. At the initial time, the assimilation experiments have no storm information at all. Starting at 30 min, available pseudo observations are assimilated into the model, followed by a short

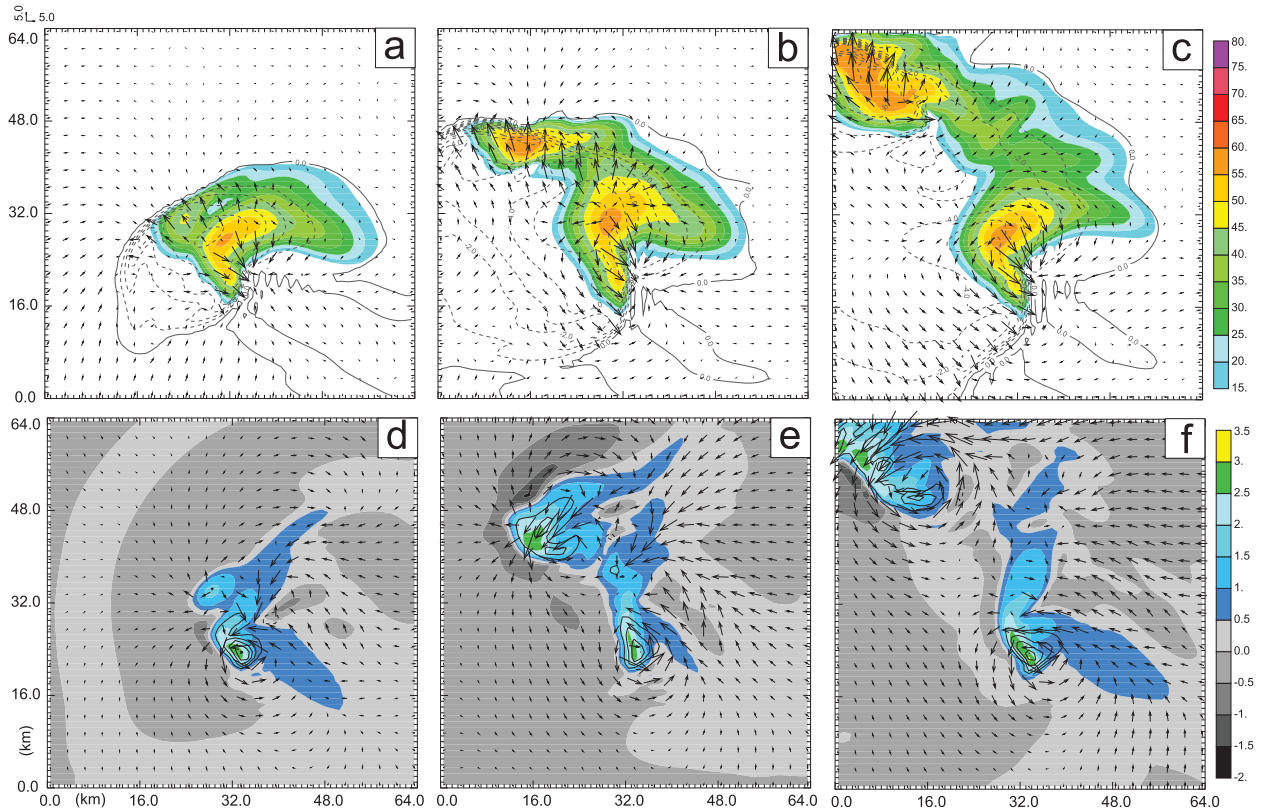


FIG. 1. (a)–(c) The quantities \mathbf{V}'_h (vectors), θ' (contours every 1 K), and reflectivity (shaded) at $z = 250$ m AGL. (d)–(f) \mathbf{V}'_h (vectors), w (contours every 6 m s^{-1}), and q'_i (shaded) at $z = 5$ km AGL from the simulation run every 30 min from 50 to 110 min into the truth simulation. (a),(d) $t = 50$ min; (b),(e) $t = 80$ min; (c),(f) $t = 110$ min.

forecast (the length of which is varied in different experiments); this assimilation-forecast cycle is repeated until 120 min (a 90-min assimilation period).

A total of 36 data assimilation experiments are performed; 12 experiments for each of 3 different assimilation frequencies (Table 2). For each set of 12 experiments, the first 5 assimilate only one type of observations, and are intended to examine 1) how the model responds to the assimilation of different types of observations, and 2) which type of observations exert greater impact on the model analysis. The next four experiments assimilate horizontal wind components and one more type of observations. The last three experiments assimilate both horizontal and vertical wind components and one more type of observations. The goal of the latter seven experiments is to examine the impact of assimilating observations in different combinations. Each experiment is named by listing the types of observations assimilated followed by the assimilation time interval, separated by an underscore. For example, experiment VhWpt_5 assimilates \mathbf{V}_h , w , and θ every 5 min. In these names, the first letter of each variable is capitalized and θ is replaced by Pt.

To evaluate the performance of different observing system simulation experiments (OSSEs), we compute

RMS error statistics of the model variables between the experiments and the truth simulation as follows (Ge et al. 2010):

$$\text{RMS}_{V_h} = \sqrt{\frac{\sum_{i=1}^N (u - u_{\text{simu}})_i^2 + \sum_{i=1}^N (v - v_{\text{simu}})_i^2}{2N}}, \quad (3)$$

and

$$\text{RMS}_s = \sqrt{\frac{\sum_{i=1}^N (s - s_{\text{simu}})_i^2}{N}}, \quad (4)$$

TABLE 1. Standard deviations of observation error σ_o and background error σ_b .

	σ_o	σ_b
\mathbf{V}_h (m s^{-1})	1	3
w (m s^{-1})	0.667	2
θ (K)	0.667	2
q_v (g kg^{-1})	0.25	0.75
q_r (g kg^{-1})	0.1	0.3

TABLE 2. The list of experiments assimilating measurements, their corresponding SRT (minutes), ASED, and RMSZ (dBZ) at the end of 90-min data assimilation.

Obs	Every minute			Every 5 min			Every 10 min		
	SRT	ASED	RMSZ	SRT	ASED	RMSZ	SRT	ASED	RMSZ
\mathbf{V}_h	32	0.001	0.3	70	0.067	4.1		0.210	6.7
w	84	0.141	4.7		0.706	12.6		0.934	20.1
θ		1.963	11.4		0.847	12.6		0.896	17.6
q_v		0.180	6.94		0.371	7.3		0.587	9.4
q_r		1.402	5.1		1.268	11.4		0.891	14.3
VhW	29	0.002	0.4	36	0.004	0.9	71	0.076	3.6
VhPt	30	0.038	1.7	28	0.042	2.1	43	0.057	5.2
VhQv	19	0.018	2.0	18	0.008	1.5	25	0.020	2.0
VhQr	29	0.004	2.7	46	0.025	2.1	81	0.101	3.6
VhWPt	27	0.018	0.7	24	0.030	1.2	31	0.105	2.8
VhWQv	18	0.028	2.8	20	0.006	1.3	21	0.008	1.4
VhWQr	25	0.008	2.7	27	0.007	1.5	51	0.037	2.5

where N is the total number of grid points used in the calculation; u and v are the horizontal wind components in x and y directions, respectively; s stands for scalar model variable; and subscript $simu$ indicates data from the truth simulation. In this study, we compute RMS error statistics for \mathbf{V}'_h , w , θ' , q'_v , and q_r , which can be regarded as five performance indices. The change of these indices over time can be used to illustrate how different model fields evolve during the assimilation process.

To make the performance evaluation more convenient, we compute the energy difference (ED), following Fabry and Sun (2010), between the experiments and the truth simulation. Three types of energy differences are defined here—the kinetic energy difference (KED), the thermal energy difference (TED), and the latent energy difference (LED):

$$\text{KED} = \frac{1}{2} \int_D (\Delta u^2 + \Delta v^2 + \Delta w^2) dD, \quad (5)$$

$$\text{TED} = \frac{c_p}{2T_r} \int_D \Delta T^2 dD, \quad (6)$$

and

$$\text{LED} = \frac{L_p^2}{2c_p T_r} \int_D \Delta q_v^2 dD, \quad (7)$$

where D stands for the integration domain, $\Delta(\cdot)$ indicates a difference calculation, c_p is the specific heat, L is the latent heat of vaporization, and T_r is a reference temperature of 270 K, chosen following Ehrendorfer and Errico (1995). Fabry and Sun (2010) computed the summation of all ED terms. Similarly, we compute the summation of KED, TED, and LED; we note, however, that KED dominates the sum, limiting the effectiveness

of the summation for evaluating and delineating the experiments when considering dynamic, thermodynamic, and precipitation structures together. For this reason we introduce scaled EDs (i.e., SKED, STED, and SLED) computed by dividing the EDs by their respective values at the beginning of the data assimilation period. The average of the three scaled EDs (ASED) is then used as an index to evaluate the accuracy of analyzed storms.

For hydrometeors, it is hard to define an ED similar to those described above. In this study, we use the RMS error in simulated reflectivity (RMSZ) as a proxy index for the difference in rainwater mixing ratio between the experiments and the truth simulation. This index is straightforward because the simulated reflectivity directly shows the location, shape, and structure of the storms. Used together, ASED and RMSZ provide a convenient and efficient basis for comparing the performance of different assimilation experiments.

To measure how quickly different experiments successfully recover the simulated storms, successfully recovery time (SRT) is defined as the length of time required for an experiment to achieve scaled EDs of less than 0.2 and an RMSZ of less than 10 dBZ. To measure how accurate the recovered storms are at the end of data assimilation, ASED and RMSZ at the final analysis time are computed and compared among different experiments. It should be noted that when calculating the RMS errors and EDs, only grid points that are located in cloudy regions, defined as regions where simulated reflectivity ≥ 10 dBZ, are included.

3. Results of experiments

In this study, 12 data assimilation experiments are conducted for each assimilation frequency (every 1, 5,

and 10 min). Hence, there are a total of 36 data assimilation experiments. For each experiment, the SRT, final ASED, and final RMSZ are determined according to the criteria described in the previous section; the results are listed in Table 2. When SRT is left blank, this indicates that the “successful recovery” criteria were not met during the assimilation period.

a. Experiments assimilating a single type of observations

The experiments assimilating a single type of observations are suitable for investigating the response of the model, initialized from a cold start, to the assimilation of individual type of observations. In these experiments, starting from the analysis of the first cycle (i.e., at the beginning of data assimilation window), a 5-min-long forecast is launched and the model state is output at each time step (i.e., every 6 s) to allow for a close examination. In the following subsections we will focus on the model responses from cold start to different types of observations, as well as addressing and comparing the impacts of different types of observations. We will focus here on experiments using the 5-min assimilation frequency; results obtained using other assimilation frequencies will be discussed later.

1) ASSIMILATING HORIZONTAL WINDS

When both horizontal wind components are assimilated, vertical velocity, potential temperature, and water vapor mixing ratio are the model fields that are most strongly impacted during the first assimilation cycle. In Fig. 2, horizontal wind divergence (DIV), vertical velocity w , perturbation potential temperature θ' , and perturbation water vapor mixing ratio q'_v from experiment Vh_5 are shown at 4 km AGL at 0, 6, 12, and 300 s after the first observations are assimilated. At $t = 0$ s, the assimilation of horizontal wind observations produces horizontal wind divergence/convergence (Fig. 2a); meanwhile w , θ' , and q'_v remain practically unchanged (Figs. 2b–d). After one integration time step ($t = 6$ s), DIV decreases (Figs. 2e vs 2a). At the same time, an updraft center with a maximum value of 6.277 m s^{-1} and several weaker downdraft centers appear in the w field (Fig. 2f). The updraft and downdraft centers are collocated with convergence and divergence centers, respectively (cf. Fig. 2a). At $t = 6$ s, θ' and q'_v fields remain virtually unchanged (Figs. 2g,h). After one more integration time step ($t = 12$ s), weak perturbations start to appear in θ' and q'_v fields (Figs. 2k,l). As the model integrates forward further, θ' and q'_v further increase and become more organized while DIV and w decrease and become less organized (Figs. 2o,p vs 2m,n).

From this examination of the changes to the model fields immediately following the first analysis, we can conclude that, from a cold start, the model responds to the assimilation of horizontal wind observations by producing horizontal wind convergence–divergence. This initial convergence and divergence induces updrafts and downdrafts that, once established, perturb the potential temperature and water vapor fields. As the model integrates forward, the magnitude of perturbations of the horizontal winds and vertical velocity decrease while those of perturbation water vapor and perturbation potential temperature fields increase.

Such data impact is reinforced as new horizontal wind observations are assimilated into the model in subsequent data assimilation cycles. The adjustments to dynamic and thermodynamic fields resulting from assimilation of horizontal wind observations will eventually induce convection and precipitation.

In Fig. 3, perturbation horizontal winds, perturbation potential temperature, and radar reflectivity at $z = 250$ m AGL, as well as perturbation horizontal winds, vertical velocity, and perturbation water vapor fields at 5 km AGL are shown at 20, 50, and 80 min after the start of data assimilation (i.e., 50, 80, and 110 min after initialization of the truth simulation). After four assimilation cycles (20 min into the assimilation), small areas of precipitation have appeared (Fig. 3a). The vertical velocity and water vapor fields have also been partially reconstructed (Fig. 3d). As the assimilation cycles continue, the precipitation becomes stronger and spreads to wider areas (Fig. 3b), and the vertical velocity and perturbation water vapor fields become closer to those of the truth simulation (Figs. 3e vs 1e). After 80 min of assimilation of horizontal wind observations, the recovered storm cells closely resemble those of the truth simulation in terms of temperature (Fig. 3c, contours), reflectivity (Fig. 3c, shaded), vertical velocity (Fig. 3f, contours), and water vapor fields (Fig. 3f, shaded). According to the SRT criterion defined earlier, the dynamic, thermodynamic, and precipitation structures of the storms are successfully retrieved after 70 min of assimilation.

Supplemental experiments (not shown) were conducted assimilating measurements of only one of the horizontal wind components (either u or v). The model response in these supplemental experiments is similar to that in Vh_5. However, the magnitude of response is much smaller and assimilating only one component cannot successfully recover storm structures after 90 min of cycled data assimilation. This result may be related to the limited ability of the 3DVAR to directly “retrieve” nonobserved wind components when only one component is measured; in such cases more advanced methods such as 4DVAR or EnKF may perform better.

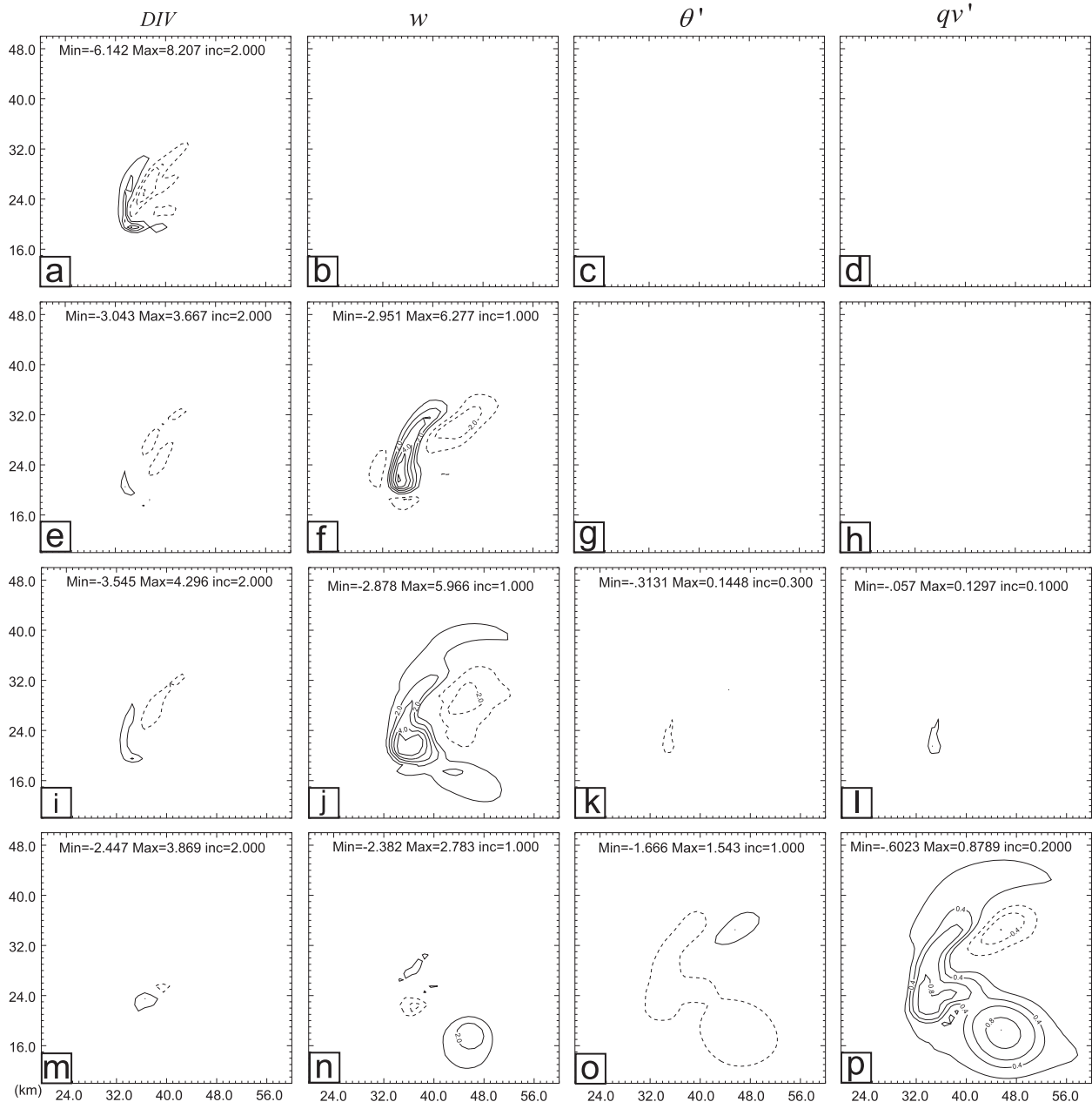


FIG. 2. (left to right) The horizontal wind divergence field, vertical velocity, perturbation potential temperature, perturbation water vapor mixing ratio for experiment Vh_5 at $z = 4$ km AGL. (a)–(d) At $t = 0$ s into the assimilation run; (e)–(h) at $t = 6$ s into the assimilation run; (i)–(l) at $t = 12$ s into the assimilation run; (m)–(p) at $t = 300$ s into the assimilation run. (k), (l) Contour intervals are different that those in (o), (p). The horizontal axis starts from 20 km and the vertical axis starts from 10 km.

2) ASSIMILATING VERTICAL VELOCITY

When w observations are assimilated into the model at the first assimilation cycle, other model fields are perturbed by the upward or downward advection induced by the assimilated w observations as model integrates forward (not shown). Warm, moist air from near the

surface is brought upward, eventually reaching saturation, resulting in condensation. Other dynamic and thermodynamic fields in the model adjust accordingly. As with the assimilation of horizontal wind observations, this data impact is reinforced in subsequent data assimilation cycles.

Figure 4 shows the perturbation horizontal winds, perturbation potential temperature, and radar reflectivity at

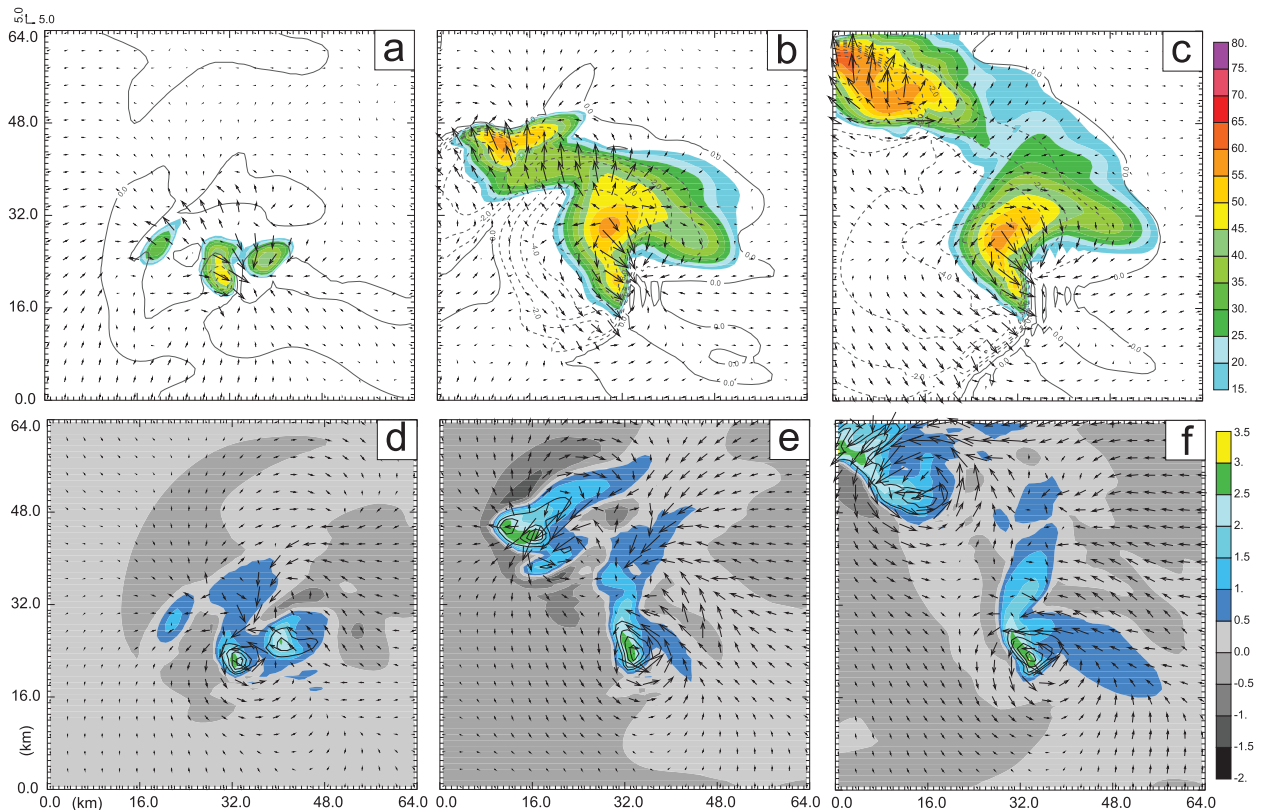


FIG. 3. As in Fig. 1, but for experiment Vh_5 every 30 min from 20 to 80 min into the assimilation run (corresponding to 50–110 min into the truth simulation). (a),(d) $t = 20$ min; (b),(e) $t = 50$ min; (c),(f) $t = 80$ min.

250 m AGL, and perturbation horizontal winds, vertical velocity, and perturbation water vapor fields at 5 km AGL at 20, 50, and 80 min after the start of data assimilation (i.e., 50, 80, and 110 min of model time in the truth simulation). In terms of reflectivity, the storm cell near the center of domain is recovered reasonably well by the end of the assimilation window (Fig. 4c). The water vapor field (Fig. 4f) for the dominant cell is very similar to that of the truth simulation. The storm cell in the northwest corner of the model domain is also partially rebuilt.

On the other hand, noticeable discrepancies still exist in the horizontal wind (Figs. 4c,f, vectors), perturbation potential temperature (Fig. 4c, contours), and perturbation water vapor (Fig. 4f, shaded) fields, especially for the northwest storm. Furthermore, the reflectivity pattern for the northwest storm is not very similar to that of the truth simulation. Using the SRT criterion, this experiment fails to achieve a successful recovery.

3) ASSIMILATING POTENTIAL TEMPERATURE

When θ observations are assimilated, the direct impact on the model is to adjust the buoyancy; these changes to buoyancy subsequently induce vertical motion. As

integration continues, horizontal wind and water vapor fields change accordingly, and rainfall is gradually produced with further assimilation cycles.

In Fig. 5, perturbation horizontal winds, perturbation potential temperature, and radar reflectivity at $z = 250$ m AGL and perturbation horizontal wind, vertical velocity, and perturbation water vapor fields at $z = 5$ km AGL are shown 20, 50, and 80 min after the start of data assimilation. Near the end of assimilation window, the recovered reflectivity (Fig. 5c) is comparable to that of the truth simulation (Fig. 1c). Both storm cells are correctly located and are relatively accurate in terms of intensity. However, some differences from the truth run remain in areas with reflectivity between 15 and 25 dBZ. The mid- to upper-level wind and water vapor fields (Fig. 5f) are also substantially different from the truth simulation (Fig. 1f). Near the end of the assimilation window, the horizontal wind circulation around the northwest storm cell differs greatly from that of the truth simulation (Figs. 5f vs 1f, vectors). Several spurious water vapor areas are produced (Fig. 5f, shaded), and updraft cores are weaker than those in the truth simulation and are wrongly oriented (Figs. 5f vs 1f, contours).

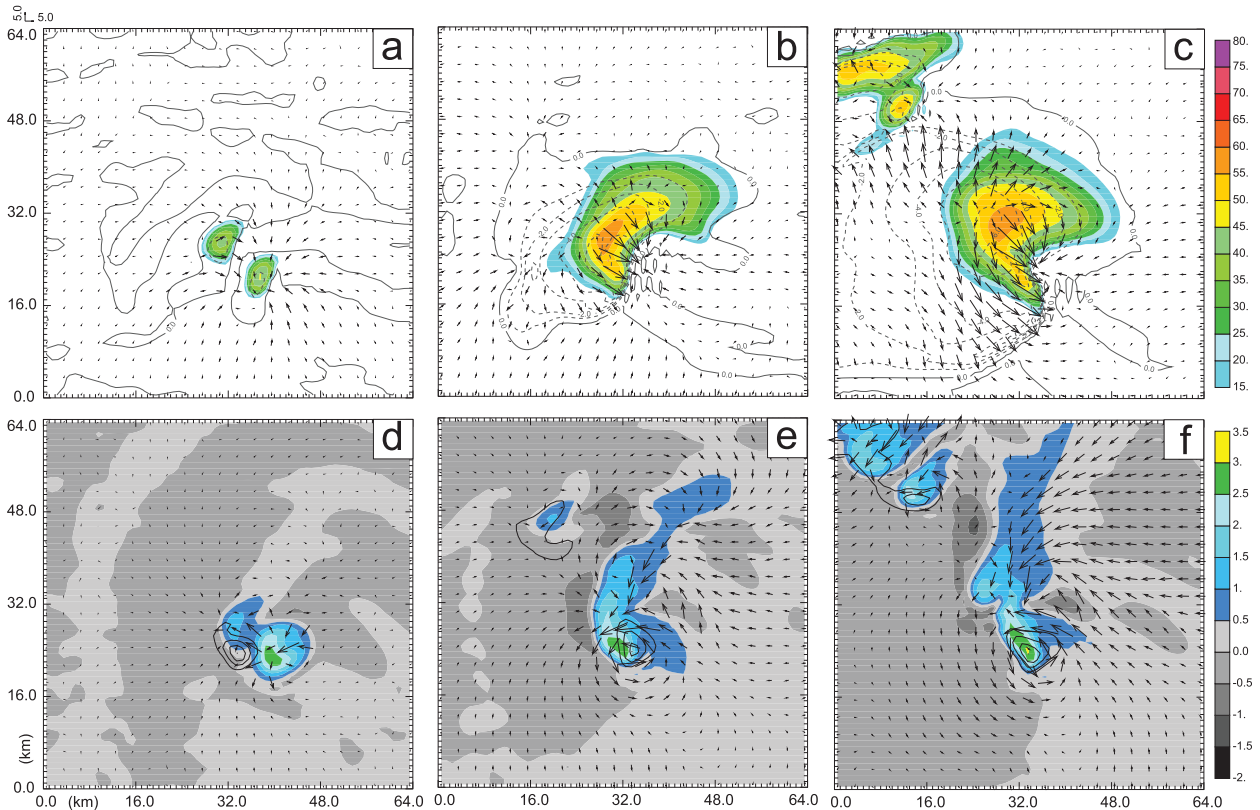


FIG. 4. As in Fig. 3, but for experiment W_5.

The RMS error statistics from experiment Pt_5 are presented in Fig. 6. The impact of assimilating θ observations is primarily seen in the recovery of the storm precipitation structure. The vertical velocity field is only partially recovered, and the horizontal wind and water vapor fields are poorly retrieved. Overall, this experiment also fails to recover the simulated thunderstorms after 90 min of intermittent data assimilation.

4) ASSIMILATING WATER VAPOR

When q_v observations are assimilated into the model at the beginning of data assimilation window, the initial response in the model is the production of cloud water (Fig. 7h) through condensation, which heats the air (Fig. 7f). The change in buoyancy due to perturbations in the water vapor field is another cause of model response but this effect is much smaller. This can be confirmed by Fig. 7g, which shows little change in the vertical velocity. A scale analysis (not shown) of the buoyancy terms indicates that the contribution to buoyancy from perturbation of the water vapor field is on the order of 0.01 m s^{-2} near the storm center; in contrast, the contribution of perturbation potential temperature is on the order of 0.1 m s^{-2} . Therefore, the direct buoyancy response from

the assimilation of q_v observations is rather small compared to the impact of induced condensation and associated latent heating. The changed temperature induces vertical motion in the w field in subsequent integration time steps (Fig. 7k). As the model continues to integrate forward, more condensation and latent heating are produced (Figs. 7n,p) and w increases in magnitude.

The recovery of reflectivity is quite successful in this experiment (Fig. 8). As early as at 50 min (Fig. 8b) into the assimilation period, the reflectivity pattern has become very similar to that of the truth simulation. Near the end of the assimilation window (Fig. 8c), the reflectivity pattern is even closer to the truth. The final RMS error for simulated reflectivity at 90 min into the assimilation is 7.3 dBZ, well below the 10-dBZ maximum error level set by the SRT criterion. Recovery of the temperature field is also successful. The cold pool is reasonably reestablished around both storm cells (Fig. 8c), with location and coverage similar to those in the truth simulation. On the other hand, the mid- to upper wind fields are not well recovered even at the end of the assimilation period (Fig. 8f). The wind circulations around the storm cells (Fig. 8f, vectors) are not as strong as those in the truth simulation (Fig. 1f, vectors). The updraft cores

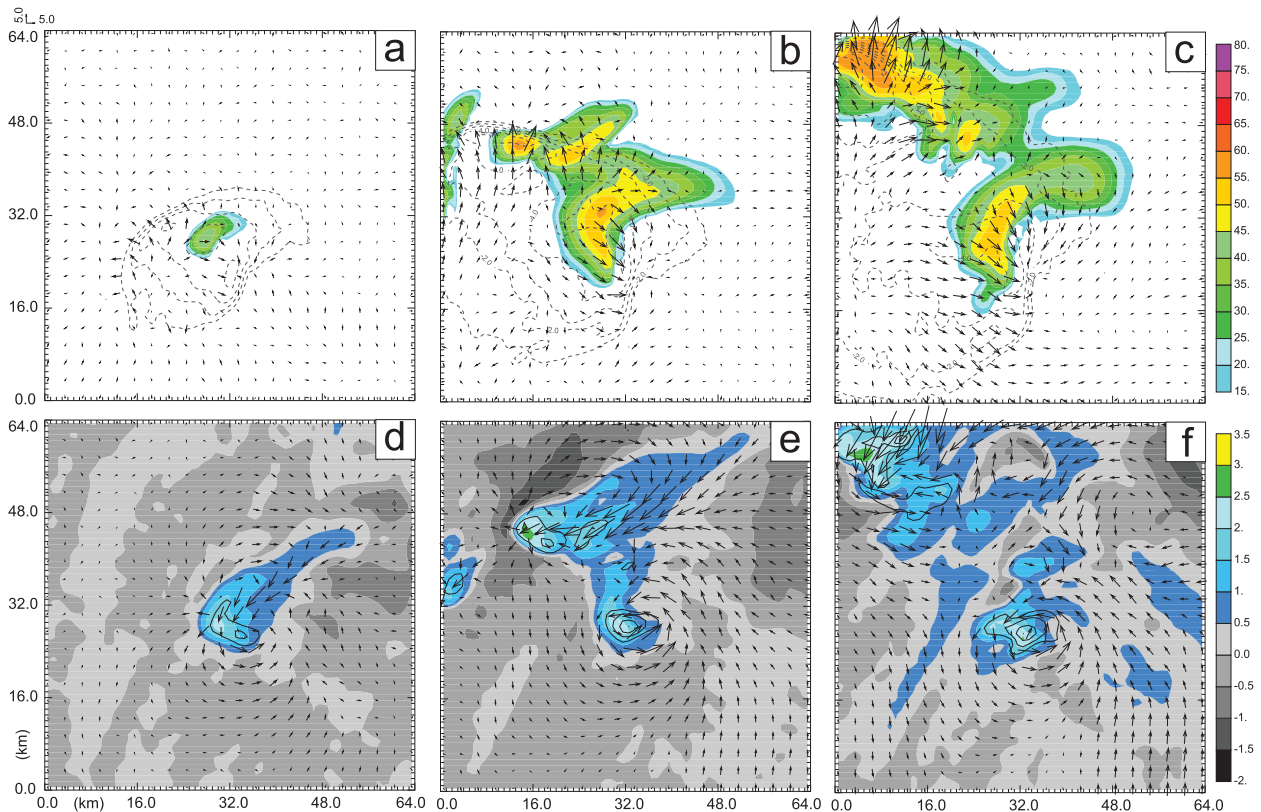


FIG. 5. As in Fig. 3, but for the experiment Pt_5.

(Fig. 8f, contours) are also wrongly oriented compared to the truth simulation (Fig. 1f, contours). This poor performance in retrieving the wind fields, especially the horizontal wind fields, can also be inferred from the very limited decrease in the RMS errors for horizontal wind fields (Fig. 9). Therefore, using the SRT criterion, this experiment fails to successfully recover the simulated thunderstorms.

5) ASSIMILATING RAINWATER

When q_r observations are assimilated, the major impact on the model is to change the buoyancy through water loading, leading to the development of downward vertical motion (Figs. 10e,h). Evaporative cooling is another noticeable impact (Figs. 10f,i), which also tends to induce downdrafts. The wind and water vapor fields subsequently adjust in response to these processes.

With continued assimilation of q_r observations, the cold pool is rebuilt well (Figs. 11b,c), although notable differences remain in its strength and distribution. The mid- to upper-level temperature field (not shown), however, is not retrieved well. The surface horizontal winds are too strong along the gust front (Figs. 11c vs 1c, vectors), and mid- to upper-level circulation centers and the updraft cores are located incorrectly (Figs. 11f vs 1f,

vectors and contours). The water vapor field is also very different from the truth simulation (Figs. 11f vs 1f, shaded). Using the SRT criterion, this experiment also fails to successfully recover the simulated thunderstorms.

6) SUMMARY

Among the experiments assimilating a single type of observations at 5-min intervals, only experiment Vh_5 successfully recovers the simulated thunderstorms, having a SRT of 70 min (see Table 2). At the end of the data assimilation window, Vh_5 yields a very low ASERD (0.067) and RMSZ (4.1 dBZ); these values are much smaller than those of experiments W_5, Pt_5, Qv_5, and Qr_5. These results indicate that the assimilation of horizontal wind components have the largest impact on the supercell storm analysis and short-range forecast. This conclusion is consistent with the findings of Weygandt et al. (1999), Sun (2005), and Nascimento and Droegemeier (2006), all of whom found that horizontal winds play a key role in the evolution of convective storms. Weygandt et al. (2002b) also found that the prediction of a supercell thunderstorm is most sensitive to the perturbation horizontal velocity. Park and Droegemeier (2000), Fabry and Sun (2010), and Fabry (2010) demonstrated that errors in temperature and moisture fields have the

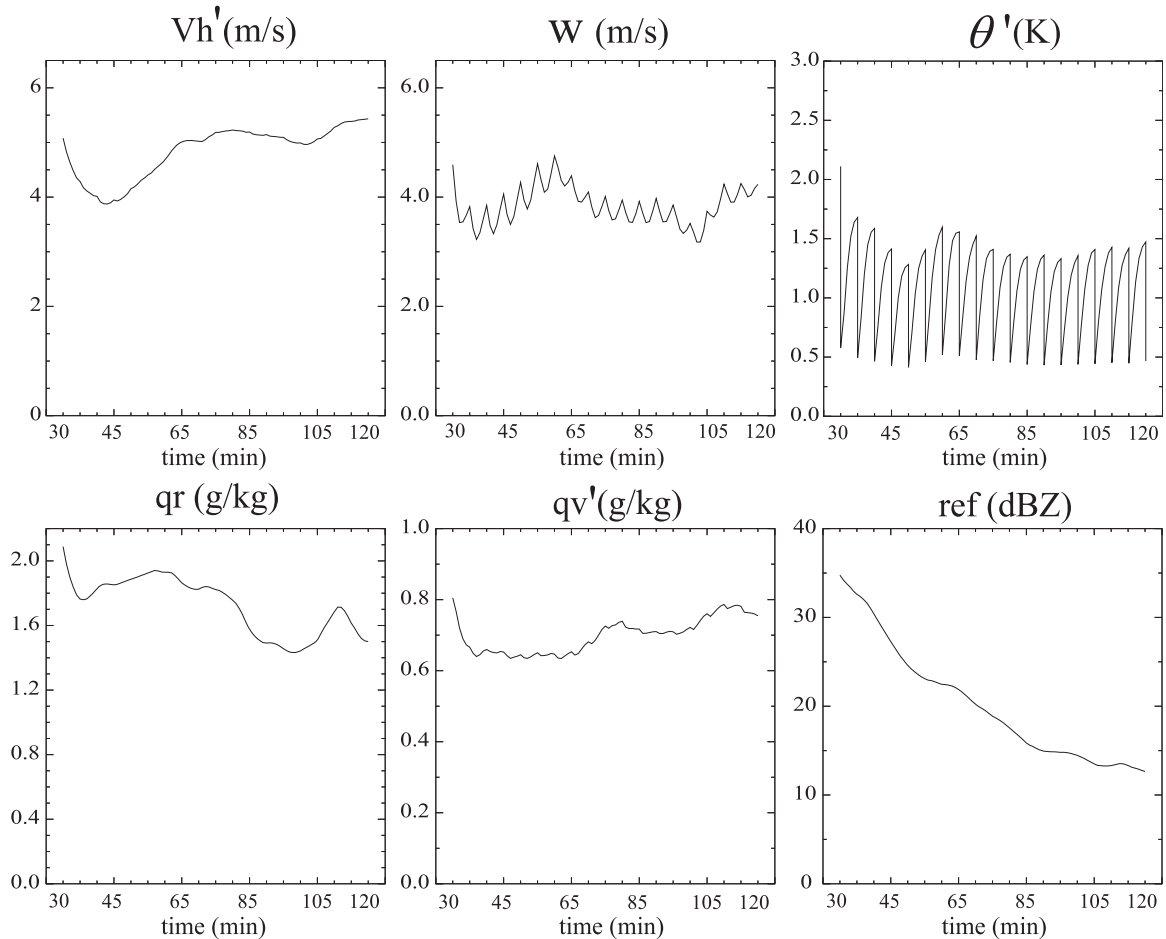


FIG. 6. The RMS errors of analyses (at 5-min intervals) and of forecasts every minute for experiment Pt_5 for (top, left to right) V_h' , w , θ' and (bottom, left to right) q_r , q_v' , and reflectivity. The horizontal axis shows the minutes into the truth run.

greatest impact on the quality of the forecast. The focus of these studies is on the error propagation from the initial condition; this topic is beyond the scope of this study. However, it is a very important issue and merits further study in the future.

Among the other experiments (W_5, Pt_5, Qv_5, and Qr_5) that assimilate w , θ , q_v , or q_r data individually without horizontal winds, Qv_5 yields the smallest ASED (0.371) and RMSZ (7.3 dBZ), suggesting that water vapor is the second most important type of observation for accurate retrieval. A similar conclusion was drawn in Sun (2005); furthermore, Weygandt et al. (2002a,b) also indicate that a simulated supercell storm is strongly affected by the water vapor field. Observations of q_v are very effective in rebuilding the precipitation field, and to some extent the thermodynamic fields, but they are poor at recovering wind fields. Observations of w are the third most important for a successful retrieval, as indicated by the ASED and RMSZ statistics of experiment W_5 compared to Pt_5 and

Qr_5. Observations of q_r have the least impact; when q_r is assimilated alone, the result is poorly recovered dynamic and thermodynamic structures. It should be noted that limited impact of the q_r observations may be due to the fact that the assimilation of q_r does not have a direct impact on temperature and moisture fields in the 3DVAR analysis. In a system where temperature and moisture fields are adjusted directly by q_r observations through q_r observations may have more impact (e.g., a semi-empirical cloud analysis procedure, or as a result of using a more advanced data assimilation method such as 4DVAR or EnKF).

b. Experiments assimilating horizontal wind components and one more type of observations

Experiment Vh_5 yields a SRT of 70 min (Table 2), indicating that assimilation of horizontal wind components alone is effective for storm retrieval. The 70 min required for Vh_5 to reach a successful recovery, however, is quite long considering the life cycle of a typical

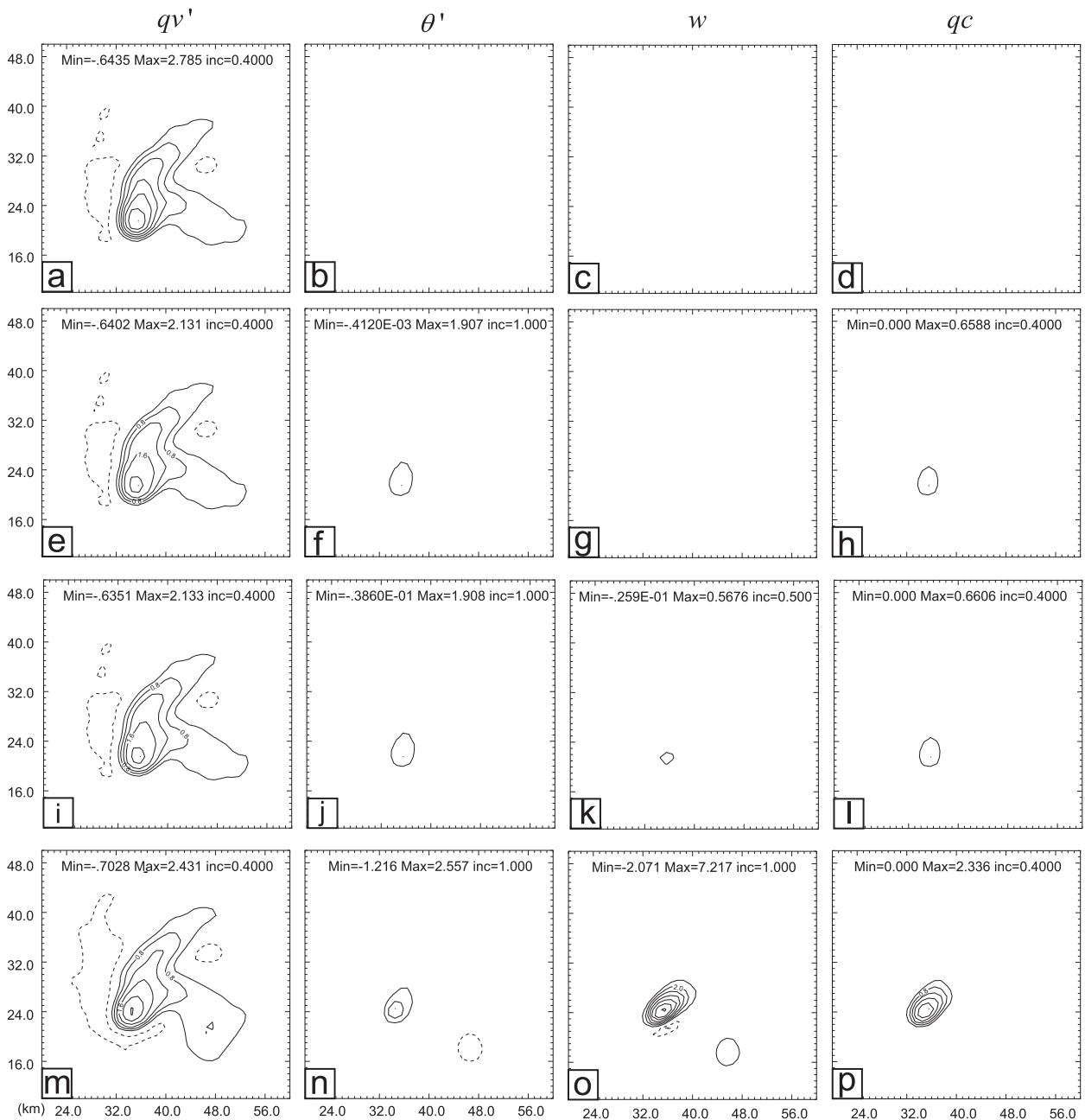
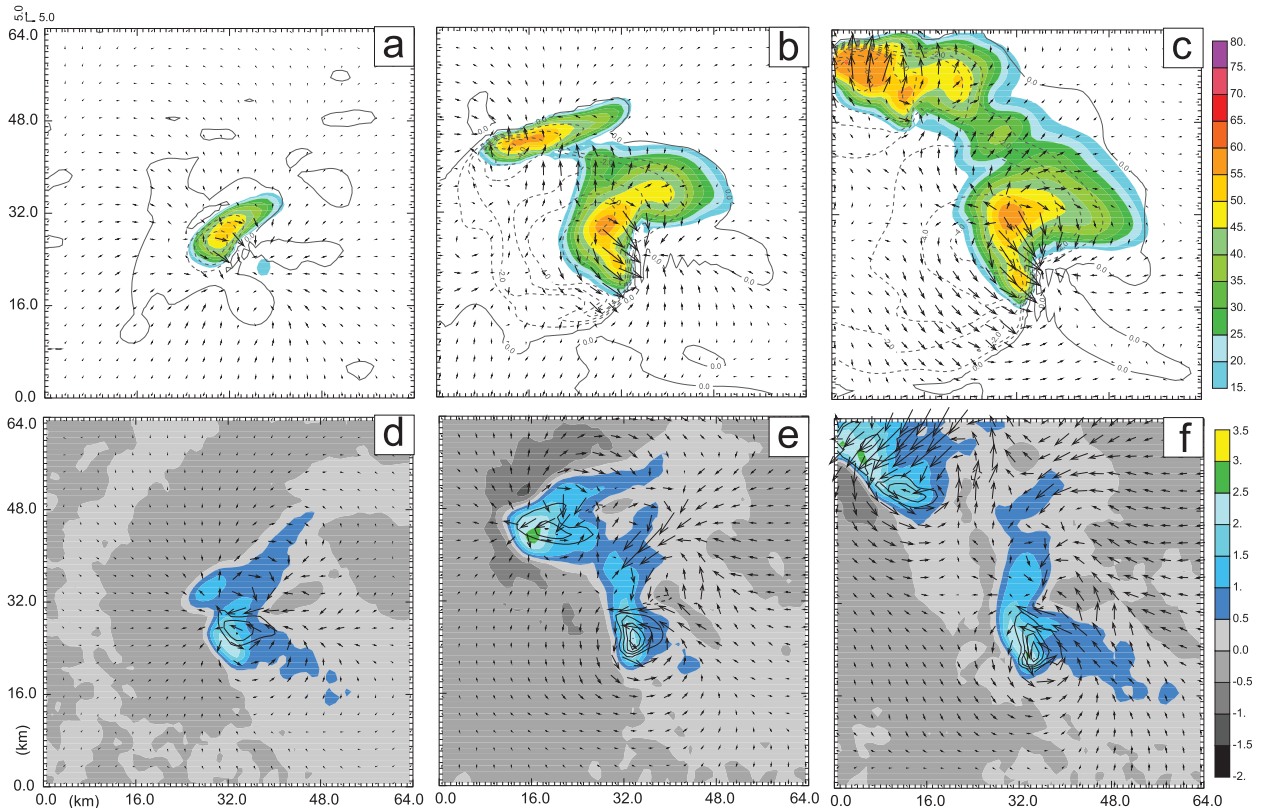


FIG. 7. As in Fig. 2, but for the perturbation water vapor mixing ratio, perturbation potential temperature, vertical velocity, and cloud water mixing ratio for experiment Qv_5.

convective storm and the operational need for quick delivery of storm-scale forecasts.

Assimilating one more type of observations in addition to horizontal wind components may help alleviate this problem. Table 2 lists SRT for experiments assimilating horizontal winds and one other type of observations. All such experiments reduce the SRT compared to Vh_5: VhW_5 has an SRT of 36 min; VhPt_5, 28 min; VhQv_5, 18 min; and VhQr, 46 min. These results

confirm that assimilating another type of observations alongside the horizontal wind can accelerate the successful recovery of simulated storms, when measurements are assimilated every 5 min. Similar results were obtained in Tong and Xue (2005), Hu et al. (2006b), and Zhao and Xue (2009), where the assimilation of radar reflectivity data in addition to radial velocity data was found to improve storm-scale data assimilation results.

FIG. 8. As in Fig. 3, but for experiment Qv_5 .

Among VhW_5 , $VhPt_5$, $VhQv_5$, and $VhQr_5$, experiment $VhQv_5$ yields the smallest SRT (28 min). This again confirms that water vapor measurements are the second most important type of observation after horizontal wind measurements. With the availability of horizontal winds, additional θ observations result in faster recovery than additional w observations (SRT of 28 min for $VhPt_5$ vs 36 min for VhW_5). The finding that temperature observations add more useful information to the analysis than observations of the vertical wind can be attributed to the fact that the vertical velocity is more closely correlated to horizontal wind divergence than temperature; therefore, the latter offers more independent information.

Experiment $VhQr_5$ yields the largest SRT of 46 min among VhW_5 , $VhPt_5$, $VhQv_5$, and $VhQr_5$. This further confirms that q_r observations have less impact than q_v , w , and θ observations on the storm-scale analyses performed in this study.

c. Experiments assimilating all three wind components and one more type of observations

The experiment that assimilates all three wind components yields a SRT of 36 min, which is much smaller

than when assimilating only the horizontal wind components (Vh_5 has an SRT of 70 min). This indicates that for storm-scale data assimilation, efforts should be made to obtain measurements of all three wind components that are as accurate as possible. Experiments $VhWpt_5$, $VhWQv_5$, and $VhWQr_5$ all perform better than VhW_5 in terms of SRT, suggesting that assimilating one more type of observations in addition to the three wind components can further improve data assimilation results. Among those three experiments, $VhWQv_5$ has the smallest SRT value and $VhWQr_5$ has the largest one, again confirming that after the horizontal wind measurements, water vapor is the next most important type of observation and q_r is the least important.

d. Impacts of assimilation frequency

The experiments assimilating observations every 5 min all have smaller SRTs than the corresponding experiments assimilating the same types of observations every 10 min (Table 2). As expected, the model performs better when more observations are assimilated. When model variables are updated more frequently, the model state variables are impacted more strongly by the observations, the data impacts are usually better maintained, and the

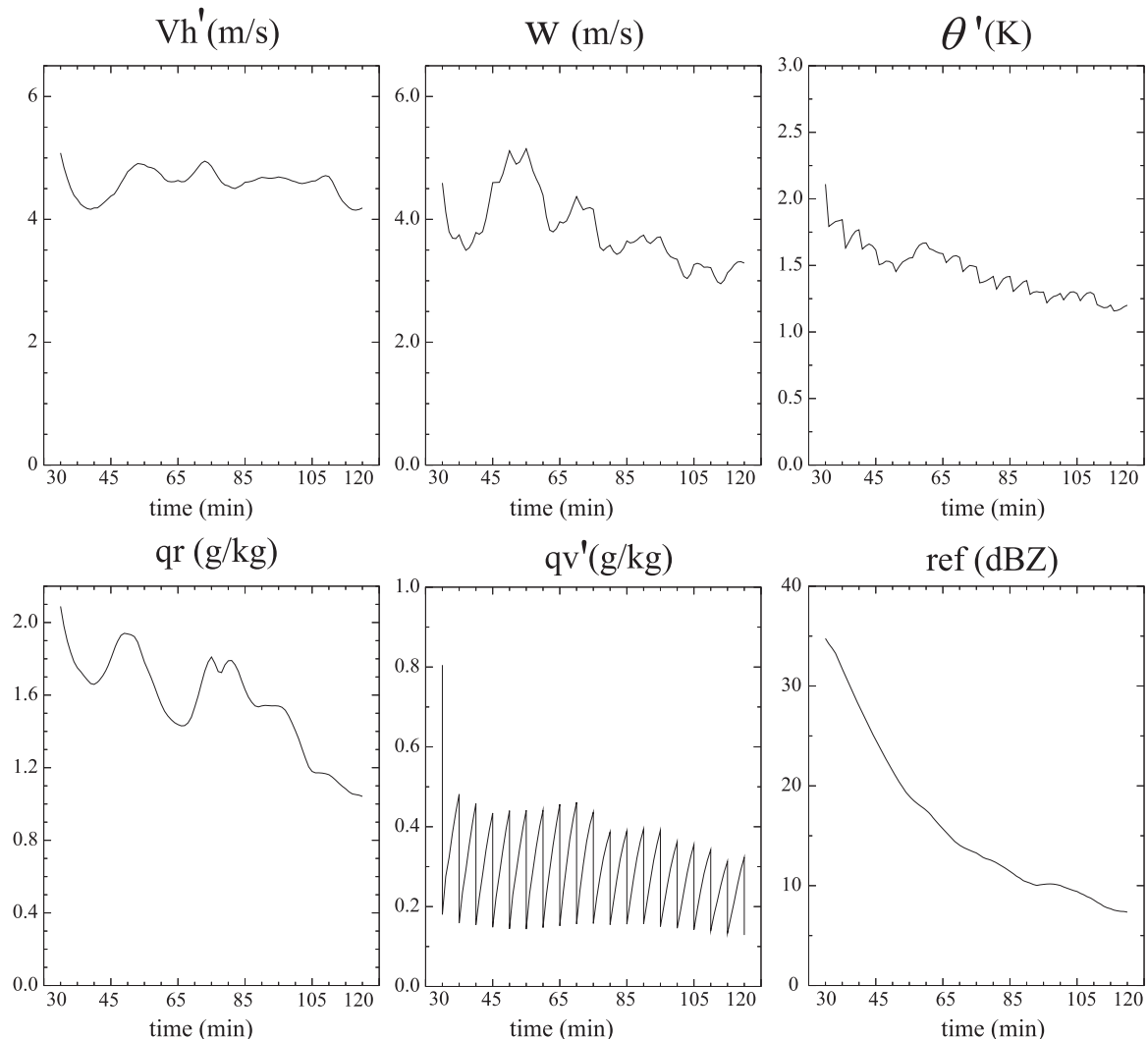


FIG. 9. As in Fig. 6, but for experiment Qv_5.

model storms are recovered in a shorter time. This finding is consistent with the results of Zhang et al. (2004), Xue et al. (2006), and Hu and Xue (2007), which also examined, using either EnKF or 3DVAR, the impacts of assimilation frequency on the analysis of convective storms. Zhang et al. (2004) found that more frequent observations (every 2 min vs every 5 min) improved the data assimilation in the early stage (first half-hour) although the benefit diminished later in the assimilation period. Xue et al. (2006) showed that faster radar volume scans (faster than 5-min intervals) can improve the quality of the analysis. Hu and Xue (2007) reported that assimilation at 5-min intervals yielded better analyses and forecasts than assimilation at 10-min intervals.

The above findings naturally lead to a question: since a higher assimilation frequency can produce better results, should we therefore assimilate observations at the

highest frequency possible (e.g., every model time step at which data are available) in order to obtain better analyses? Our experiments suggest that, in practice, assimilating data with extremely high frequency is not necessarily desirable. Assimilating observations every minute does not result in substantial improvement over assimilating observations every 5 min (Fig. 12 and Table 2). The SRTs of VhWQv_1 and VhWQr_1 are only 2 min shorter than the corresponding SRTs of VhWQv_5 and VhWQr_5. Such a small improvement does not merit the greatly increased costs in computation and data collection required to obtain and assimilate observations at 1-min intervals. Moreover, VhPt_1 and VhWpt_1 actually have somewhat larger SRTs than VhPt_5 and VhWpt_5 as a result of larger LED values (whose computation is based on the water vapor field) in VhPt_1 and VhWpt_1 than VhPt_5 and VhWpt_5.

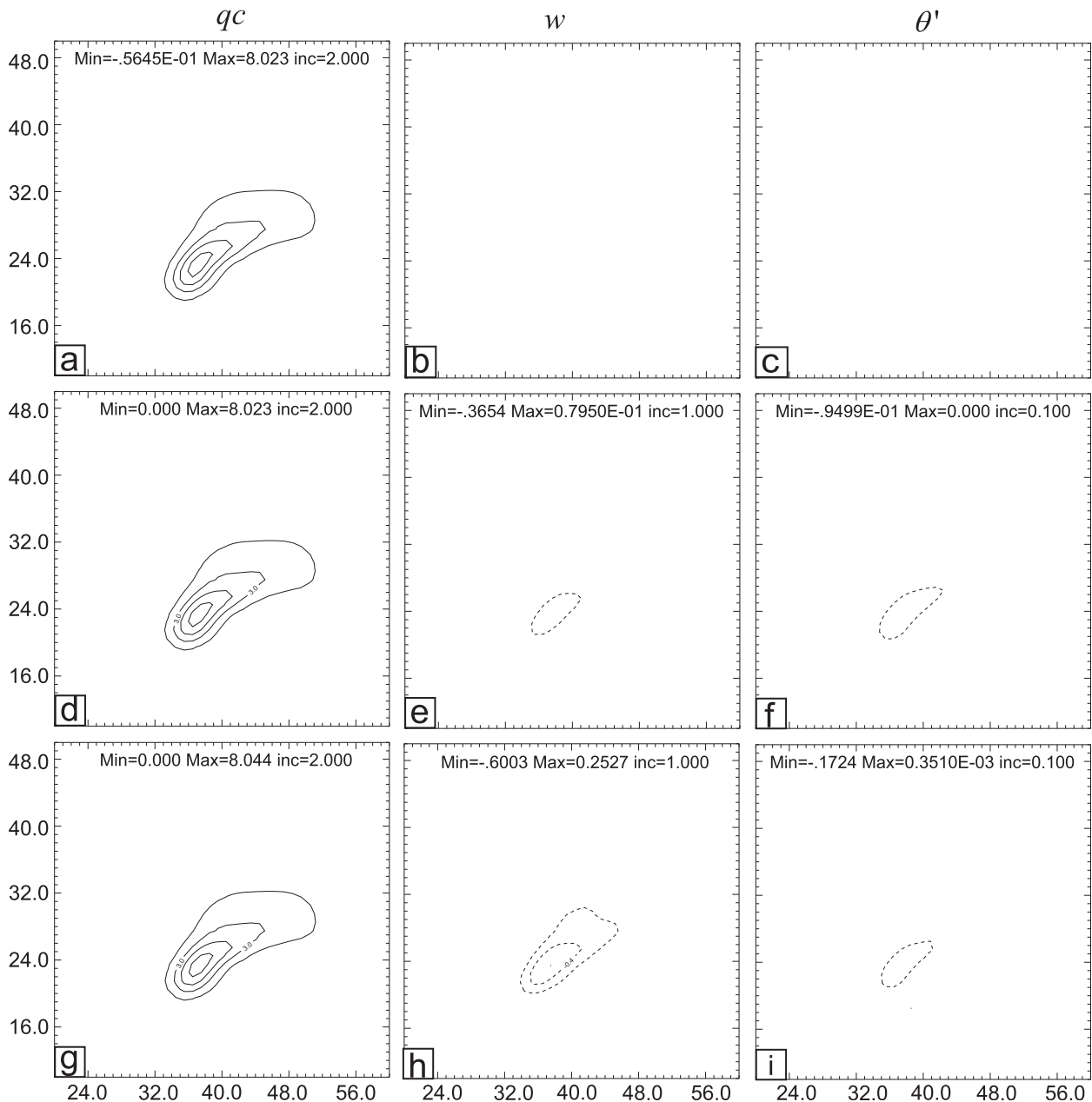


FIG. 10. (left to right) The rainwater mixing ratio, vertical velocity, and perturbation potential temperature from experiment Qr_5, at $z = 4$ km AGL. (a)–(c) At $t = 0$ s into the assimilation run; (d)–(f) at $t = 6$ s into the assimilation run; (g)–(i) at $t = 12$ s into the assimilation run. The horizontal axis starts from 20 km and the vertical axis starts from 10 km.

We attribute this behavior to the following: the pseudomeasurements of potential temperature are assumed to be available at the grid points and they contain added random noise. When assimilated into the model very frequently, the increased noise level can have a negative impact on the precipitation forecast. The model needs time to adjust and damp out such noise. One minute of model integration may be insufficient for the model to completely remove the noise. These results suggest that,

in some situations (as with temperature measurements in this case), assimilating observations too frequently may hurt the analysis. On the other hand, experiments assimilating \mathbf{V}_h and/or w observations every minute show benefits from the more frequent assimilation, suggesting that it is generally beneficial to assimilate wind observations often.

In section 3b, we noted that assimilating another type of observations in addition to horizontal wind components

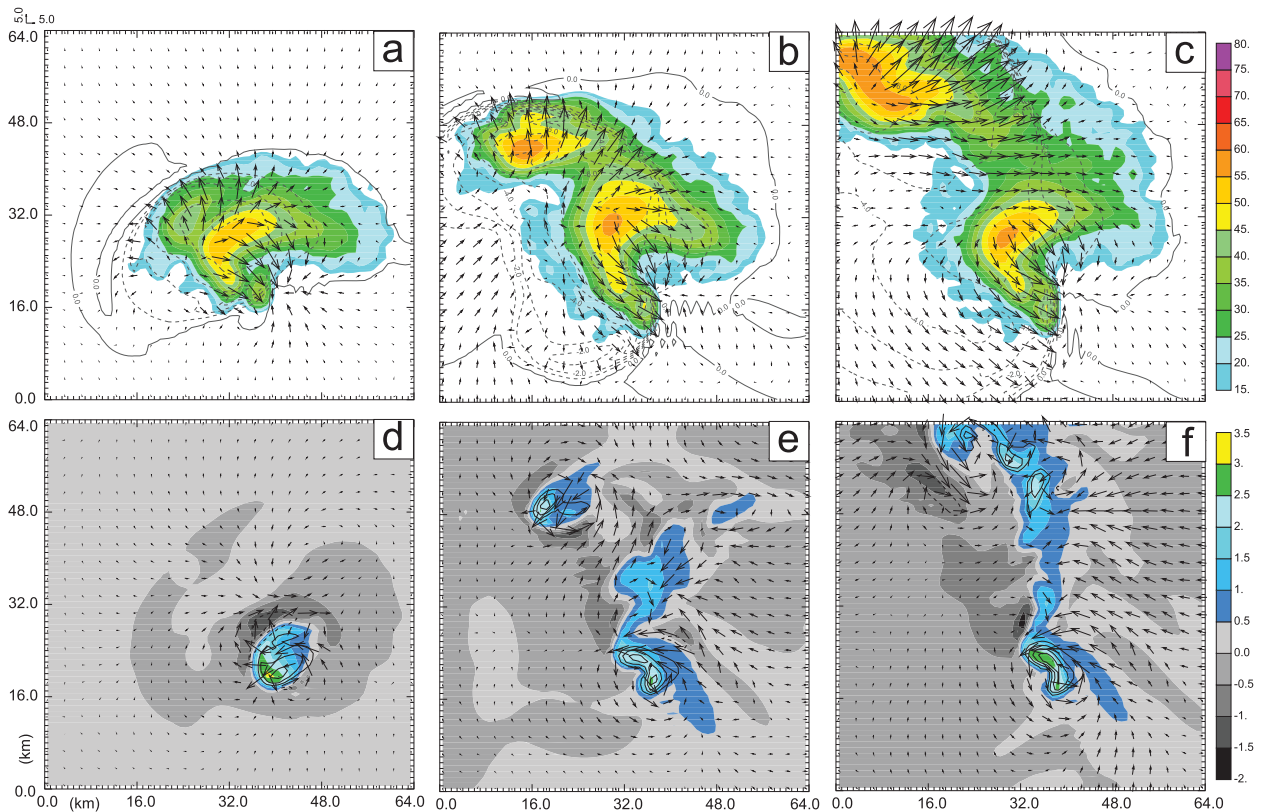


FIG. 11. As in Fig. 3, but for experiment Qr_5.

can accelerate the successful recovery of simulated storms when measurements are assimilated every 5 min. The same conclusion can be drawn when assimilating data every 10 min (see Table 2). However, when assimilating observations every minute, the SRTs from VhW_1, VhPt_1, and VhQr_1 are not much reduced compared to Vh_1. The ASEDs and RMSZs from those three experiments increase slightly compared to Vh_1. At the same time, the SRT of VhQv_1 is smaller than that of Vh_1. Therefore, when assimilating horizontal wind observations every minute, the benefits from using an additional type of observations are not evident except for water vapor observations. This is presumably because assimilating wind observations at 1-min intervals is already very effective in recovering the model storm; additional measurements thus have only a small effect. This is also true when all three wind components are assimilated; little additional improvement is obtained when the three wind components are already assimilated at a 1-min interval.

4. Summary and conclusions

In this study, we examined the impacts of assimilating measurements of different state variables and the impacts

of data assimilation frequency through a series of OSSEs using a three-dimensional variational data assimilation system. Different types of pseudo-observations are assimilated into a storm-scale NWP model individually or in various combinations. The model responses (from a cold start) to the assimilation of individual types of

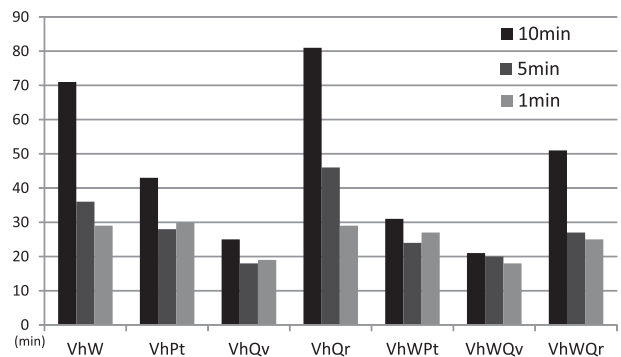


FIG. 12. Bar chart of the SRT values from experiments assimilating two and three types of measurements. The vertical axis shows the SRT values in minutes; the horizontal axis shows different observation combinations. For each observation combination, three bars are plotted, which represents the SRT values (left to right) from 10-, 5-, and 1-min assimilation interval experiments, respectively.

observations are investigated in detail to help us understand the impacts of the different observation types. A criterion for “successful recovery” of the storm is defined using the energy difference and the RMS error of simulated radar reflectivity between the assimilation run and truth run. When met, this criterion indicates that the dynamic, thermodynamic, and precipitation structures of the storm in the analysis are sufficiently close to those in the truth simulation. The criterion is used to evaluate the performance of different data assimilation experiments so that the impacts of different types of observations and assimilation frequencies can be quantified.

The primary model response to the assimilation of horizontal wind observations is to force vertical motions through horizontal wind divergence/convergence, which in turn induces temperature and humidity perturbations through upward and downward motions. In subsequent assimilation cycles, storm dynamic and thermodynamic structures are spun up gradually. When vertical velocity observations are assimilated, other model variables are directly perturbed by the upward and downward advection. Temperature, humidity and precipitation fields can then be recovered to some extent in subsequent assimilation cycles, but the horizontal wind components are poorly recovered. When potential temperature observations are assimilated, the direct adjustment in the model is change of the air buoyancy, inducing vertical motion. Precipitation fields can be spun up to some extent, but the horizontal wind, vertical velocity, and humidity fields are retrieved very poorly. When the model assimilates water vapor observations, cloud water is produced through condensation and heating is resulted from latent heat release. The changed temperature then induces vertical motion. This makes water vapor observations effective at reconstructing temperature, precipitation and, to some extent, vertical velocity fields, but ineffective at recovering horizontal winds. For rainwater observations, which lack a direct impact on the temperature and moisture fields in the 3DVAR analysis, the direct influence is limited to changing the air buoyancy through water loading and subsequent evaporative cooling, enhancing downdrafts. As a result, the rainwater observations can help establish the correct precipitation field and cold pool, but are poor at rebuilding storm dynamic and thermodynamic structures. Earlier studies using the ARPS 3DVAR system to assimilate reflectivity data through an empirical cloud analysis scheme, which includes in-cloud temperature adjustments (e.g., Hu et al. 2006a) showed a much larger impact of the radar reflectivity data. Similar results are found when reflectivity data is assimilated using an EnKF method in which temperature and moisture fields are adjusted through flow-dependent cross covariance (e.g., Tong and

Xue 2005). Using a 4DVAR system, the assimilation of q_r data also tends to have a greater impact (e.g., Sun and Crook 1997).

Among all types of measurements, horizontal wind observations have the greatest impact on the storm analyses and short-range forecasts in this study; assimilation of horizontal wind observations is very effective at recovering other model fields. Therefore, in practice, considerable effort should be made to obtain as many wind observations as possible with the highest accuracy possible. One way this can be achieved through the assimilation of radial velocity measurements from multiple Doppler radars. Schenkman et al. (2011) and Snook et al. (2011, 2012) showed that assimilating multiple Center for Collaborative and Adaptive Sensing of the Atmosphere (CASA) radar radial velocity data in addition to Weather Surveillance Radar-1988 Doppler (WSR-88D) data improves analyses and forecasts of a mesoscale convective system. The finding also suggests that importance of further developing advanced velocity retrieval schemes from single- or multiple-Doppler radar data. For example, Shapiro et al. (2009) reported that including a vorticity equation constraint in a 3D variational framework could improve dual-Doppler wind analyses.

The impact of water vapor observations is the second largest. Currently, obtaining storm-scale water vapor observations is a difficult task. However, some water vapor information can be derived from near-surface refractivity measurements by radars (Fabry et al. 1997; Bodine et al. 2010); these data have been successfully assimilated into NWP models (Gasperoni et al. 2013). In the future, water vapor information may be available at high resolution because of the advances in the observing systems such as next-generation GOES satellites and dense ground-based GPS receiver networks (Wolfe and Gutman 2000; Liu and Xue 2006; Ho et al. 2007; Liu et al. 2007). The assimilation of such dense observations is expected to significantly improve storm-scale NWP.

The relative importance of vertical velocity and potential temperature measurements is somewhat dependent on data assimilation frequency. When assimilating data every minute, vertical velocity observations exert a larger impact than potential temperature observations. On the other hand, when assimilated every 5 or 10 min, potential temperature observations are more effective than vertical velocity observations. Rainwater observations show the least impact.

The impact of data assimilation frequency is also examined. In general, the assimilation frequency has a substantial impact on the quality of the resulting convective storm analysis. In this study, results obtained

using 1-, 5-, and 10-min assimilation intervals are compared. When assimilating horizontal wind observations every 5 or 10 min, including additional types of observations in the assimilation process will improve the analysis and subsequent short-range forecast. However, when the horizontal wind observations or all three wind components are assimilated every minute, the benefits from additional observation types become negligible except for water vapor measurements. This appears to be because the results from assimilating the wind components at such a high frequency are already very good; additional observations, therefore, cannot impart much further help. For measurements of horizontal wind, vertical velocity, rainwater, or their combinations, 1-min assimilation frequency produces the best results. For measurements of potential temperature, water vapor, or a combination of these measurements with wind measurements, 1-min data assimilation frequency does not produce better analysis than 5-min frequency. The time needed for the model to adjust and damp out noise introduced by the frequent assimilation is believed to be the cause.

While the above findings can provide guidance for the design and/or improvement of storm-scale observing systems and storm-scale data assimilation practice, and the key findings appear to be consistent with findings obtained using the more advanced EnKF data assimilation method, we do note that the conclusions obtained here are based on simulations of a single idealized supercell storm using a particular univariate data assimilation method. Whether these conclusions apply to other cases and other data assimilation methods requires further study. In the future, the experiments presented in this study can be repeated with the more sophisticated version of the ARPS 3DVAR system, which includes equation constraints designed to couple dynamic and thermodynamic fields (Ge et al. 2012), and also a cloud analysis package designed to help spread rainwater information to temperature and moisture fields. Similar studies could also be carried out using more advanced assimilation methods, such as EnKF and 4DVAR.

Acknowledgments. This research was supported by NSF Grants ATM-0738370, ATM-0802888, and NOAA's Warn-on-Forecast project. Computations were performed at the Pittsburgh Supercomputing Center (PSC) and Oklahoma Supercomputing Center for Research and Education (OSCER). The third author acknowledges the support of NSF Grants OCI-0905040, AGS-0941491, AGS-1046171, and AGS-1046081, and National 973 Fundamental Research Program of China (2013CB430103). The authors also thank Dr. Nathan Snook for proofreading the manuscript. Thoughtful comments from two

anonymous reviewers and Editor Dr. Fuqing Zhang significantly improved this paper.

REFERENCES

- Bodine, D., P. L. Heinselman, B. L. Cheong, R. D. Palmer, and D. Michaud, 2010: A case study on the impact of moisture variability on convection initiation using radar refractivity retrievals. *J. Appl. Meteor. Climatol.*, **49**, 1766–1778.
- Ehrendorfer, M., and R. M. Errico, 1995: Mesoscale predictability and the spectrum of optimal perturbations. *J. Atmos. Sci.*, **52**, 3475–3500.
- Fabry, F., 2010: For how long should what data be assimilated for the mesoscale forecasting of convection and why? Part II: On the observation signal from different sensors. *Mon. Wea. Rev.*, **138**, 256–264.
- , and J. Sun, 2010: For how long should what data be assimilated for the mesoscale forecasting of convection and why? Part I: On the propagation of initial condition errors and their implications for data assimilation. *Mon. Wea. Rev.*, **138**, 242–255.
- , C. Frush, I. Zawadzki, and A. Kilambi, 1997: On the extraction of near-surface index of refraction using radar phase measurements from ground targets. *J. Atmos. Oceanic Technol.*, **14**, 978–987.
- Gao, J.-D., M. Xue, K. Brewster, and K. K. Droegemeier, 2004: A three-dimensional variational data analysis method with recursive filter for Doppler radars. *J. Atmos. Oceanic Technol.*, **21**, 457–469.
- Gasperoni, N. A., M. Xue, R. D. Palmer, and J. Gao, 2013: Sensitivity of convective initiation prediction to near-surface moisture when assimilating radar refractivity: Impact tests using OSSEs. *J. Atmos. Oceanic Technol.*, in press.
- Ge, G., J. Gao, K. Brewster, and M. Xue, 2010: Impacts of beam broadening and earth curvature on storm-scale 3D variational data assimilation of radial velocity with two Doppler radars. *J. Atmos. Oceanic Technol.*, **27**, 617–636.
- , —, and M. Xue, 2012: Diagnostic pressure equation as a weak constraint in a storm-scale three dimensional variational radar data assimilation system. *J. Atmos. Oceanic Technol.*, **29**, 1075–1092.
- Hayden, C. M., and R. J. Purser, 1995: Recursive filter objective analysis of meteorological fields: Applications to NESDIS operational processing. *J. Appl. Meteor.*, **34**, 3–15.
- Ho, S., Y. Kuo, and S. Sokolovskiy, 2007: Improvement of the temperature and moisture retrievals in the lower troposphere using AIRS and GPS radio occultation measurements. *J. Atmos. Oceanic Technol.*, **24**, 1726–1739.
- Hu, M., and M. Xue, 2007: Impact of configurations of rapid intermittent assimilation of WSR-88D radar data for the 8 May 2003 Oklahoma City tornadic thunderstorm case. *Mon. Wea. Rev.*, **135**, 507–525.
- , —, and K. Brewster, 2006a: 3DVAR and cloud analysis with WSR-88D level-II data for the prediction of Fort Worth tornadic thunderstorms. Part I: Cloud analysis and its impact. *Mon. Wea. Rev.*, **134**, 675–698.
- , —, J. Gao, and K. Brewster, 2006b: 3DVAR and cloud analysis with WSR-88D level-II data for the prediction of Fort Worth tornadic thunderstorms. Part II: Impact of radial velocity analysis via 3DVAR. *Mon. Wea. Rev.*, **134**, 699–721.
- Kessler, E., 1969: *On the Distribution and Continuity of Water Substance in Atmospheric Circulations*. *Meteor. Monogr.*, No. 32, Amer. Meteor. Soc., 84 pp.

- Liu, H., and M. Xue, 2006: Retrieval of moisture from slant-path water vapor observations of a hypothetical GPS network using a three-dimensional variational scheme with anisotropic background error. *Mon. Wea. Rev.*, **134**, 933–949.
- , —, R. J. Purser, and D. F. Parrish, 2007: Retrieval of moisture from simulated GPS slant-path water vapor observations using 3DVAR with anisotropic recursive filters. *Mon. Wea. Rev.*, **135**, 1506–1521.
- Lorenc, A. C., 1986: Analysis methods for numerical weather prediction. *Quart. J. Roy. Meteor. Soc.*, **112**, 1177–1194.
- Nascimento, E. L., and K. K. Droegemeier, 2006: Dynamic adjustment in a numerically simulated mesoscale convective system: Impact of the velocity field. *J. Atmos. Sci.*, **63**, 2246–2268.
- Park, S. K., and K. K. Droegemeier, 2000: Sensitivity analysis of a 3D convective storm: Implications for variational data assimilation and forecast error. *Mon. Wea. Rev.*, **128**, 140–159.
- Purser, R. J., and R. McQuigg, 1982: A successive correction analysis scheme using recursive numerical filters. British Meteorological Office Tech. Note 154, 17 pp.
- Ray, P. S., B. C. Johnson, K. W. Johnson, J. S. Bradberry, J. J. Stephens, K. K. Wagner, R. B. Wilhelmson, and J. B. Klemp, 1981: The morphology of severe tornadic storms on 20 May 1977. *J. Atmos. Sci.*, **38**, 1643–1663.
- Schenkman, A. D., M. Xue, A. Shapiro, K. Brewster, and J. Gao, 2011: The analysis and prediction of the 8–9 May 2007 Oklahoma tornadic mesoscale convective system by assimilating WSR-88D and CASA radar data using 3DVAR. *Mon. Wea. Rev.*, **139**, 224–246.
- Shapiro, A., C. K. Potvin, and J. Gao, 2009: Use of a vertical vorticity equation in variational dual-Doppler wind analysis. *J. Atmos. Oceanic Technol.*, **26**, 2089–2106.
- Snook, N., M. Xue, and Y. Jung, 2011: Analysis of a tornadic mesoscale convective vortex based on ensemble Kalman filter assimilation of CASA X-band and WSR-88D radar data. *Mon. Wea. Rev.*, **139**, 3446–3468.
- , —, and —, 2012: Ensemble probabilistic forecasts of a tornadic mesoscale convective system from ensemble Kalman filter analyses using WSR-88D and CASA radar data. *Mon. Wea. Rev.*, **140**, 2126–2146.
- Sun, J., 2005: Initialization and numerical forecasting of a supercell storm observed during STEPS. *Mon. Wea. Rev.*, **133**, 793–813.
- , and N. A. Crook, 1997: Dynamical and microphysical retrieval from Doppler radar observations using a cloud model and its adjoint. Part I: Model development and simulated data experiments. *J. Atmos. Sci.*, **54**, 1642–1661.
- Tong, M., and M. Xue, 2005: Ensemble Kalman filter assimilation of Doppler radar data with a compressible nonhydrostatic model: OSS experiments. *Mon. Wea. Rev.*, **133**, 1789–1807.
- Weygandt, S., P. Nutter, E. Kalnay, S. K. Park, and K. Droegemeier, 1999: The relative importance of different data fields in a numerically simulated convective storm. Preprints, *Eighth Conf. on Mesoscale Processes*, Boulder, CO, Amer. Meteor. Soc., 310–315.
- , A. Shapiro, and K. K. Droegemeier, 2002a: Retrieval of model initial fields from single-Doppler observations of a supercell thunderstorm. Part I: Single-Doppler velocity retrieval. *Mon. Wea. Rev.*, **130**, 433–453.
- , —, and —, 2002b: Retrieval of model initial fields from single-Doppler observations of a supercell thunderstorm. Part II: Thermodynamic retrieval and numerical prediction. *Mon. Wea. Rev.*, **130**, 454–476.
- Wolfe, D. E., and S. I. Gutman, 2000: Developing an operational, surface-based, GPS, water vapor observing system for NOAA: Network design and results. *J. Atmos. Oceanic Technol.*, **17**, 426–440.
- Xue, M., K. K. Droegemeier, and V. Wong, 2000: The Advanced Regional Prediction System (ARPS)—A multi-scale nonhydrostatic atmospheric simulation and prediction tool. Part I: Model dynamics and verification. *Meteor. Atmos. Phys.*, **75**, 161–193.
- , and Coauthors, 2001: The Advanced Regional Prediction System (ARPS)—A multi-scale nonhydrostatic atmospheric simulation and prediction tool. Part II: Model physics and applications. *Meteor. Atmos. Phys.*, **76**, 143–166.
- , D.-H. Wang, J.-D. Gao, K. Brewster, and K. K. Droegemeier, 2003: The Advanced Regional Prediction System (ARPS), storm-scale numerical weather prediction and data assimilation. *Meteor. Atmos. Phys.*, **82**, 139–170.
- , M. Tong, and K. K. Droegemeier, 2006: An OSSE framework based on the ensemble square root Kalman filter for evaluating impact of data from radar networks on thunderstorm analysis and forecast. *J. Atmos. Oceanic Technol.*, **23**, 46–66.
- Zhang, F., C. Snyder, and J. Sun, 2004: Impacts of initial estimate and observations on the convective-scale data assimilation with an ensemble Kalman filter. *Mon. Wea. Rev.*, **132**, 1238–1253.
- Zhao, K., and M. Xue, 2009: Assimilation of coastal Doppler radar data with the ARPS 3DVAR and cloud analysis for the prediction of Hurricane Ike (2008). *Geophys. Res. Lett.*, **36**, L12803, doi:10.1029/2009GL038658.